Article

Journal of
Nanoscience and Nanotechnology
Vol. 16, 1–5, 2016
www.aspbs.com/jnn

Enhanced Circular Dichroism of Gold Bilayered Slit Arrays Embedded with Rectangular Holes

Hao Zhang, Yongkai Wang, Lina Luo, Haiqing Wang, and Zhongyue Zhang*

School of Physics and Information Technology, Shaanxi Normal University, Xi'an 710062, China

Gold bilayered slit arrays with rectangular holes embedded into the metal surface are designed to enhance the circular dichroism (CD) effect of gold bilayered slit arrays. The rectangular holes in these arrays block electric currents and generate localized surface plasmons around these holes, thereby strengthening the CD effect. The CD enhancement factor depends strongly on the rotational angle and the structural parameters of the rectangular holes; this factor can be enhanced further by drilling two additional rectangular holes into the metal surfaces of the arrays. These results help facilitate the design of chiral structures to produce a strong CD effect and large electric fields.

Keywords: Circular Dichroism, Plasmon, Chiral Structures.

1. INTRODUCTION

Circular dichroism (CD)[1] denotes the different optical response at the origin of left-handed circularly polarized (LCP) and right-handed circularly polarized (RCP) lights. The CD effect is widely applied in broadband circular polarization,[2–4] analytical chemistry,[5] biological monitoring,[6,7] and enantiomeric sensing.[8]

Helical plasmonic structures can generate a strong CD effect given the different couplings of the oscillation strengths of electric dipoles as excited by LCP and RCP.[9] However, well-defined helical structures are difficult to prepare.[2,3,8] The CD effect can also be observed in planar and layer-by-layer chiral plasmonic structures;[10–29] in the former, CD effects are generated by breaking the chiral symmetry and inducing small-scale defects.[10–12] The electric resonant mode alone is observed in such structures under normal illuminations with circular polarization; nonetheless, the CD effect in planar structures is weak. Both electric and magnetic resonant modes can be excited in layer-by-layer structures.[13–15] In the second mode type, the two layers sustain antiparallel currents and produce local magnetic dipole moments that are mainly confined to the separation of the layers. The CD effects of layer-by-layer structures are usually stronger than those of planar structures;[13–15] therefore, the former has attracted much attention. To generate strong CD effects, researchers have recently designed bilayered rosette structures,[16] mutually twisted wires,[17–19] bilayered mutually twisted cross structures,[20,21] conjugated gammadion structures,[15,22] double-layer metallic crossed gratings,[23] bilayered twisted U-shaped structures,[24–26] and dual-layer twisted-arc structures.[27] At the resonant wavelength, the charges of the aforementioned chiral structures congregate at the endpoint of the structure and energy is transmitted to the space around the structure. As a result, energy flux congregation is reduced. By contrast, the charges of chiral plasmonic structures with slits congregate at the boundary of the slits, and the electric field is confined to these slits.[28–30] Therefore, energy distribution is concentrated. In addition, localized surface plasmons (LSP) can efficiently enhance both the electric and the magnetic fields of light. Nevertheless, the CD effect of the chiral structure with slits is weak.[28,29]

In the current study, gold bilayered slit arrays with rectangular holes (BSARH) embedded into the metal surfaces are designed to enhance the CD effect of gold bilayered slit arrays (BSA). BSARH generates a strong CD effect because the rectangular holes block electric currents and LSP are formed around these holes. The effects of rotational angle and structural parameters on the CD enhancement factor (CDEF) are determined in this work; this factor can be enhanced further by drilling two additional rectangular holes into the metal surfaces of these arrays. This study not only presents a simple method to enhance the CD effect but also contributes to the understanding of the mechanisms of this effect.

*Author to whom correspondence should be addressed.

2. STRUCTURE AND SIMULATION METHOD

Figure 1(a) shows the configuration of the BSA with embedded rectangular holes (BSARH) in the top layer. Circularly polarized (left-handed and right-handed) incident plane wave vector along the $-z$ direction normally illuminates to the proposed structure. The BSARH consists of two metal slit layers parallel to the x-y plane separated by a SiO_2 layer with refractive index of $n = 1.45$. The two metal slit layers have the same thickness of 50 nm. Rectangular hole arrays are embedded in the top layer. The centers of the rectangular holes are coincide with the centers of the overlap of two metal layers. The rectangular holes are anticlockwise rotated around their geometric centers. α represents the angle that the holes rotate from the original position. $\alpha = 0°$ denotes the case that the long side of rectangular hole is parallel to x-axis. The geometry is described by several parameters: $w_1 = 50\sqrt{2}$ nm and $w_2 = 150\sqrt{2}$ nm for the width of metal and slit, $\theta = 45°$ for the rotation of the two metal slit layers, $d = 50$ nm for the thickness of SiO_2 layer, and a and b for the width and the length of rectangular hole. The vertical view of the unit cell is rhombus, as depict in Figure 1(b). The length of the rhombus is $200\sqrt{2}$ nm.

COMSOL Multiphysics based on finite element method is used to calculate transmittance of plasmonic structures. The transmittance is defined as $T = P_{out}/P_{in}$, where P_{out} and P_{in} represent output power and incident power, respectively. The refractive index of gold is taken from Ref. [31]. We use "+" ("−") subscript denoting RCP (LCP) light. T_{++} (T_{--}) represents the transmittance of RCP (LCP) light and the CD effect is described by: $\Delta T = T_{++} - T_{--}$.[20] To quantify the CD enhancement, we introduce a scale factor, namely, the "CD enhancement factor" (CDEF). We define CDEF as the fraction of the maximum CD effect for BSARH over the maximum CD effect for BSA, i.e., $\text{CDEF} = |\Delta T|_{\text{BSARH}}/|\Delta T|_{\text{BSA}}$.

3. RESULTS AND DISCUSSION

3.1. CD of BSA and BSARH with $\alpha = 90°$

Figure 2(a) shows the transmittance spectra of BSA and BSARH when $\alpha = 90°$, $a = 30$ nm, and $b = 90$ nm under LCP and RCP illuminations. The resonant peaks are

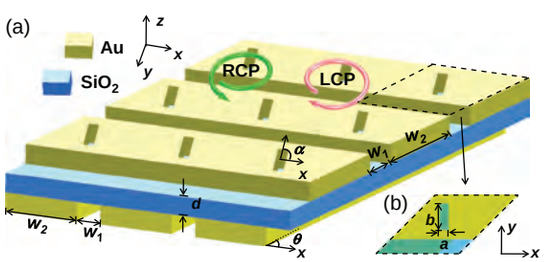

Figure 1. (a) The schematic diagram of proposed BSARH and parameters definition. (b) The vertical view of the unit cell with the associated geometric features designated in the lower-right corner.

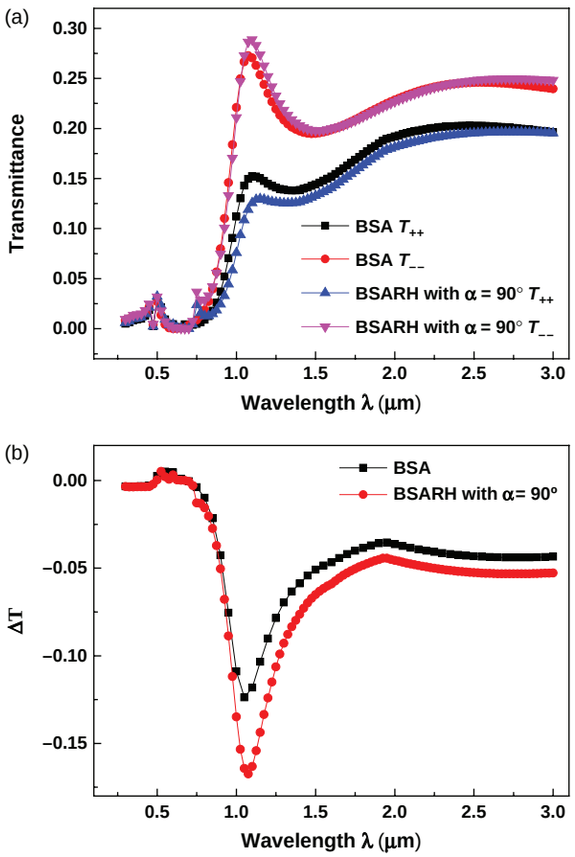

Figure 2. (a) Transmittance spectra for the BSA and BSARH with $\alpha = 90°$, $a = 30$ nm and $b = 90$ nm under RCP and LCP illuminations. (b) The CD spectra for the BSA and BSARH with $\alpha = 90°$.

observed at roughly $\lambda = 1.075$ μm and 1.100 μm for BSA and BSARH, respectively. At the resonance wavelength, the transmittance at RCP illumination (T_{++}) is lower than that at LCP illumination (T_{--}) for BSA. When one rectangular hole is embedded into the upper film, the transmittance at RCP illumination decreases, whereas that at LCP illumination increases in comparison with those of BSA. Figure 2(b) displays the CD spectra of BSA and BSARH with $\alpha = 90°$. The dips of BSA and BSARH with $\alpha = 90°$ are detected at $\lambda = 1.050$ and 1.075 μm, respectively, and the corresponding maximum transmittance differences are $|\Delta T| = 0.123$ and 0.167. Thus, CDEF = 1.36.

To elucidate the CD enhancement mechanism when a rectangular hole is drilled into the BSA, we investigate the electric field distributions and the current density at the dips in the CD spectra of BSA and BSARH with $\alpha = 90°$. The surface current directions at the bottom surface are almost parallel under LCP and RCP illuminations. Figure 3 depicts the steady-state electric field distributions and the current density at the upper surface; the red arrows represent the direction of the current. The dips in the CD spectra are attributed to the resonance between the wavelength of the surface plasmon polariton on the metal surface and

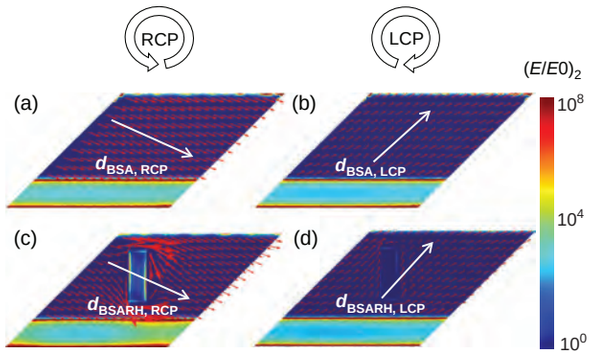

Figure 3. Simulated surface current and electric field distributions at the upper surface of the top layer for (a, b) the BSA and (c, d) the BSARH with $\alpha = 90°$ at the CD dips under RCP and LCP illuminations. Equivalent electric dipole moments are marked by white arrows and labeled by "$d_{BSA, RCP}$," "$d_{BSA, LCP}$," "$d_{SARH, RCP}$" and "$d_{BSARH, LCP}$," respectively.

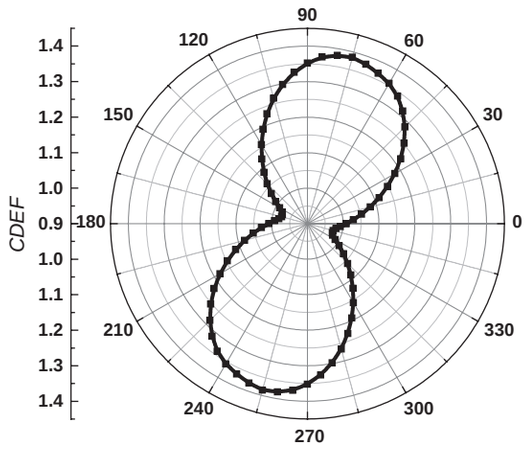

Figure 4. The polar diagram for calculated CDEFs of BSARH.

the structure period. The electron oscillations on the metal film can be regarded as effective electric dipoles, and they are marked by white arrows in Figure 3. In the middle part of the BSA upper surface, the effective electric dipoles $d_{BSA, RCP}$ move in the $-20°$ direction with respect to the x-axis under RCP illumination, as depicted in Figure 3(a). As illustrated in Figure 3(b), the effective electric dipoles $d_{BSA, LCP}$ move in the 45° direction with respect to the x-axis under LCP illumination. When a rectangular hole is drilled into the gold surface, the directions of the surface current under RCP and LCP illuminations are similar to those of $d_{BSA, RCP}$ and $d_{BSA, LCP}$, respectively, as exhibited in Figures 3(c, d). Specifically, Figure 3(c) shows that the currents are blocked by the rectangular hole under RCP illumination, and localized electric fields are generated around the side surface of this hole. These phenomena reduce the strength of the effective BSARH electric dipole $d_{BSARH, RCP}$ and limit the transmittance displayed in Figure 2(a). Figure 3(d) demonstrates that under LCP illumination, more currents flow along the side surface of the rectangular hole, which increases the strength of the effective BSARH electric dipole $d_{BSARH, LCP}$ over that of $d_{BSA, LCP}$ and enhances the transmittance presented in Figure 2(a). The different effects of the rectangular hole on the currents under RCP and LCP illuminations strengthen the CD effect of BSARH.

3.2. Dependence of α on CDEF

The rotation angle of the rectangular hole affects the effective electric dipoles of $d_{BSA, RCP}$ and $d_{BSA, LCP}$. The polar diagram for the BSARH CDEFs is calculated, as depicted in Figure 4. CDEF depends strongly on α; this factor is maximized (1.39) at $\alpha = 75°$ and minimized (0.97) at $\alpha = 160°$. Figures 5(a–d) depict the distributions of the currents and the electric fields at the upper surface of the top layer under the resonant wavelength of BSARH with $\alpha = 75°$ and $\alpha = 160°$. Figure 5(e) exhibits the geometric relationship between the directions of the currents at the upper surface of the top layer and the orientation of the rectangular hole. The direction of the current (i_{RCP}) under RCP illumination is $-20°$ with respect to the x-axis while that under LCP illumination (i_{LCP}) is 45° with respect to the x-axis. Both directions are marked by dashed lines. The orientation of the rectangular hole is denoted by red lines and is labeled as Max and Min as the CDEF is maximized and minimized. At $\alpha = 75°$, this orientation is almost perpendicular to the direction of i_{RCP}, which strengthens the LSP around the rectangular hole and strongly limits the transmittance at

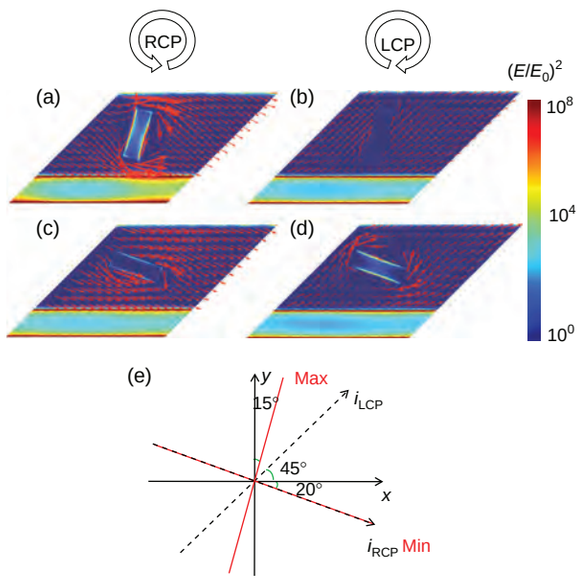

Figure 5. Simulated surface current and electric field distributions at the upper surface of the top layer for the BSARH with (a, b) $\alpha = 75°$ and (c, d) $\alpha = 160°$ at the resonant wavelength under RCP and LCP illuminations. (e) The geometric relationship between the directions of current at upper surface of the top layer and orientation of the rectangular hole.

the resonant wavelength. Thus, CDEF is maximized at $\alpha = 75°$. At $\alpha = 160°$, the orientation of the rectangular hole is parallel to the direction of the current under RCP illumination, thus weakening the LSP around the rectangular hole and minimizing CDEF. The angle generated between the current and the orientation of the rectangular hole facilitates a relationship between CDEF and α, as illustrated in Figure 4.

3.3. Dependence of α and β on CDEF

The drilled rectangular hole in upper layer leads to great CD enhancement, which also suggested us that embedding rectangular hole in the bottom layer would also be helpful for enhancing CD effect. We introduce one rectangular hole in the bottom layer, and the center of the rectangular hole is coincide with the center of the overlap of two metal layers. The rectangular hole is anticlockwise rotated around its geometric center with a certain angle β from x-axis. Figure 6(a) shows the intensity of calculated CDEFs as a function of angles α and β. The CDEF is maximized (1.72) at $\alpha = 75°$ and $\beta = 150°$ and minimized (0.97) at $\alpha = 165°$ and $\beta = 60°$. Figure 6(a) shows that the effects of α and β on CDEF are independently. Figures 6(b–e) show the surface current and electric field distributions at the bottom surface of the bottom layer for BSARH ($\alpha = 90°$) at the resonant wavelength with $\beta = 60°$ and $\beta = 150°$, respectively. At $\beta = 60°$, the directions of the currents are perpendicular to the orientation of the rectangular hole and many currents are blocked by the rectangular hole, which strengthens LSP around the rectangular hole, which decrease the intensity of effective dipole oscillation strength and results in minimum CDEF, as shown in Figures 6(b, c). At $\beta = 150°$, the direction of the current is parallel to the orientation of the rectangular hole and the currents flow along the side of the rectangular hole, which would increase the intensity of the currents and results in maximum CDEF, as exhibited in Figures 6(d, e). Therefore, when the rectangular hole drilled in the bottom layer of BSARH, the CD effect would be further enhanced.

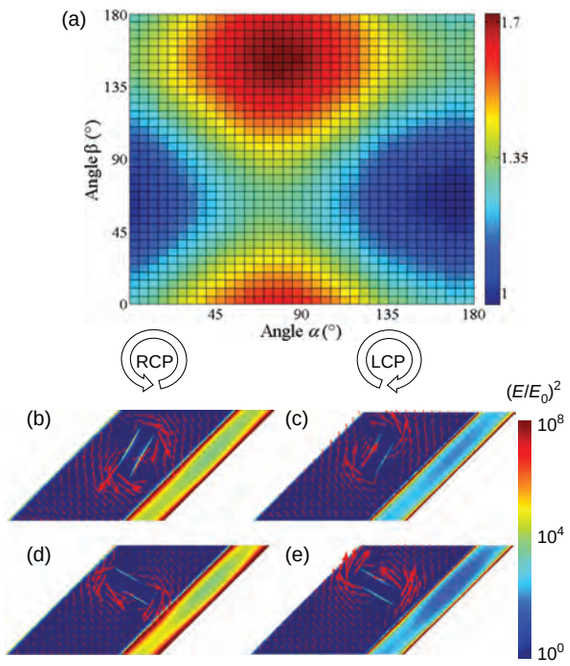

Figure 6. (a) The intensity of calculated CDEFs for BSARH as a function of angles α and β. The surface current and electric field distributions at the bottom surface of the bottom layer for BSARH ($\alpha = 90°$) at the resonant wavelength with (b, c) $\beta = 60°$ and (d, e) $\beta = 150°$ under RCP and LCP illuminations.

3.4. Dependence of the Width and Length of the Rectangular Hole on CDEF

Figure 7 shows the CDEF for BSARH as a function of a with fixed $b = 90$ nm and $\alpha = 90°$, and as a function of b with fixed $a = 30$ nm and $\alpha = 90°$, respectively. The solid curves are the fittings using exponential increase function. The CDEF is dependent on b more obviously since the currents are mainly blocked by the longer side of the rectangular hole.

3.5. Dependence of the Shapes of the Holes Embedded in the BSA on CDEF

The topological shape of the hole embedded in BSA affects CDEF as well. When circular holes with the same surface area as the rectangular holes shown in Figure 3 are drilled into the top layer of BSA, CDEF = 1.11. Figures 8(a, b) depict the current and electric field distributions at the upper surface of the top layer for the circular holes embedded in BSA at $\lambda = 1.075$ μm. Given the structural symmetry of the circular shape, the currents under RCP and LCP illuminations both flow along the side of the circle. As a result, the CDEF in this case is smaller than that of BSARH.

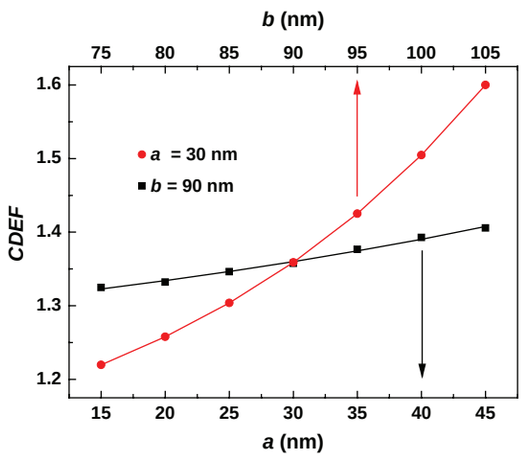

Figure 7. The CDEF for BSARH as a function of a and b. The solid curves are the fittings.

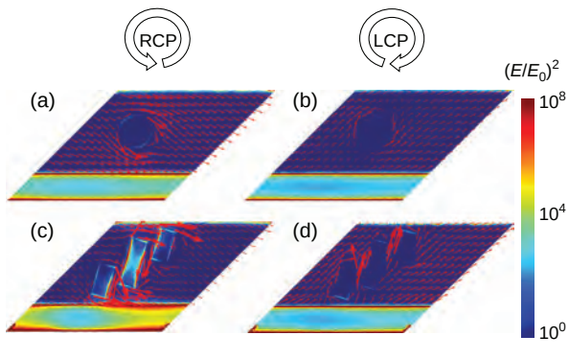

Figure 8. Simulated current and electric field distributions at the upper surface of the top layer under RCP and LCP illuminations of (a, b) BSA with circular holes drilled in the top layer and (c, d) for the BSA with three rectangular holes drilled in the top layer.

To enhance the CD effect further, two additional small rectangular holes are drilled into the upper layer of BSARH at $\alpha = 75°$. In this scenario, CDEF reaches 1.76. These two holes are both 30 nm wide and 60 nm long; moreover, they are inclined in the same direction (75° with respect to the x-axis). The centers of these holes are in the transversal extension line of the rectangular holes; the gaps are identical at 15 nm. Figures 8(c, d) display the current and electric field distributions on the upper surface of the top layer for BSA at RCP and LCP illuminations; this top layer contains three rectangular holes. As shown in Figure 8(c), the direction of the current is perpendicular to the orientation of the rectangular hole under RCP illumination; thus, many currents are blocked by the rectangular holes. Moreover, many enhanced electric fields are generated around the three holes. Under LCP illumination, the currents flow along the side of the rectangular hole, as illustrated in Figure 8(d). Thus, a large CDEF can be obtained by varying the hole structure and by introducing additional anisotropic holes.

4. CONCLUSIONS

In summary, rectangular holes are drilled into metal layers to enhance the CD effect of twist slit arrays. The embedded holes block the currents at the upper surface in different ways under RCP and LCP illuminations; thus, the CD effect of the twist slit arrays is enhanced. Moreover, CDEF depends strongly on the rotation angle and the length of the rectangular holes. Therefore, embedding rectangular holes in the bottom layer can help enhance the CD effect, which is also influenced by the topological shape of the hole embedded in BSA. This effect can be properly engineered by tuning the structural parameters, and the method of strengthening it in plasmonic structures is significant for increasing the CD signals of biological molecules.

Acknowledgments: This work was supported by the National Natural Foundation of China (Grant no. 11004160) and the Fundamental Research Funds for the Central Universities (Grant no. GK201303007).

References and Notes

1. V. K. Valev, J. J. Baumberg, C. Sibilia, and T. Verbiest, *Adv. Mater.* 25, 2517 (**2013**).
2. J. K. Gansel, M. Thiel, M. S. Rill, M. Decker, K. Bade, V. Saile, G. V. Freymann, S. Linden, and M. Wegener, *Science* 325, 650 (**2009**).
3. J. Kaschke, J. K. Gansel, and M. Wegener, *Opt. Express* 20, 26012 (**2012**).
4. X. Vidal, W. J. Kim, A. Baev, V. Tokar, H. Jee, Mark. T. Swihartad, and P. N. Prasad, *Nanoscale* 5, 10550 (**2013**).
5. F. Zhu, X. Y. Li, Y. C. Li, M. Yan, and S. Q. Liu, *Anal. Chem.* 87, 357 (**2015**).
6. W. J. Liu, D. Liu, Z. N. Zhu, B. Han, Y. Gao, and Z. Y. Tang, *Nanoscale* 6, 4498 (**2014**).
7. Y. Mochida, H. Cabral, Y. Miura, F. Albertini, S. Fukushima, K. Osada, N. Nishiyama, and K. Kataoka, *Acs Nano* 8, 6724 (**2014**).
8. M. Schäferling, D. Dregely, M. Hentschel, and H. Giessen, *Phys. Rev. X* 2, 031010 (**2012**).
9. Z. Y. Zhang and Y. P. Zhao, *Appl. Phys. Lett.* 98, 083102 (**2011**).
10. B. K. Canfield, S. Kujala, K. Laiho, K. Jefimovs, J. Turunen, and M. Kauranen, *Opt. Express* 14, 950 (**2006**).
11. H. Husu, B. K. Canfield, J. Laukkanen, B. Bai, M. Kuittinen, J. Turunen, and M. Kauranen, *Appl. Phys. Lett.* 93, 183115 (**2008**).
12. W. X. Huang, Y. Zhang, X. M. Tang, L. S. Cai, J. W. Zhao, L. Zhou, Q. J. Wang, C. P. Huang, and Y. Y. Zhu, *Opt. Lett.* 36, 3359 (**2011**).
13. M. Decker, M. W. Klein, and M. Wegener, *Opt. Lett.* 32, 856 (**2007**).
14. D. H. Kwon, P. L. Werner, and D. H. Werner, *Opt. Express* 16, 11802 (**2008**).
15. T. Cao, L. Zhang, R. E. Simpson, C. W. Wei, and M. J. Cryan, *Opt. Express* 21, 27841 (**2013**).
16. A. V. Rogacheva, V. A. Fedotov, A. S. Schwanecke, and N. I. Zheludev, *Phys. Rev. Lett.* 97, 177401 (**2006**).
17. L. Wu, Z. Y. Yang, Y. Z. Cheng, Z. Q. Lu, P. Zhang, M. Zhao, R. Z. Gong, X. H. Yuan, Y. Zheng, and J. A. Duan, *Opt. Express* 21, 5239 (**2013**).
18. J. F. Zhou, J. F. Dong, B. N. Wang, T. Koschny, M. Kafesaki, and C. M. Soukoulis, *Phys. Rev. B* 79, 121104 (**2009**).
19. Y. Zhao, M. A. Belkin, and A. Alù, *Nat. commun.* 3, 870 (**2012**).
20. J. F. Dong, J. F. Zhou, T. Koschny, and C. Soukoulis, *Opt. Express* 17, 14172 (**2009**).
21. M. Decker, M. Ruther, C. E. Kriegler, J. Zhou, C. M. Soukoulis, S. Linden, and M. Wegener, *Opt. Lett.* 34, 2501 (**2009**).
22. R. Zhao, L. Zhang, J. Zhou, T. Koschny, and C. M. Soukoulis, *Phys. Rev. B* 83, 035105 (**2011**).
23. W. S. Gao, H. M. Leung, Y. H. Li, H. Chen, and W. Y. Tam, *J. Opt.* 13, 115101 (**2011**).
24. M. Decker, R. Zhao, C. M. Soukoulis, S. Linden, and M. Wegener, *Opt. Lett.* 35, 1593 (**2010**).
25. Z. F. Li, R. Zhao, T. Koschny, M. Kafesaki, K. B. Alici, E. Colak, H. Caglayan, E. Ozbay, and C. M. Soukoulis, *Appl. Phys. Lett.* 97, 081901 (**2010**).
26. X. Xiong, W. H. Sun, Y. J. Bao, M. Wang, R. W. Peng, C. Sun, X. Lu, J. Shao, Z. F. Li, and N. B. Ming, *Phys. Rev. B* 81, 075119 (**2010**).
27. Y. H. Cui, L. Kang, S. F. Lan, S. Rodrigues, and W. S. Cai, *Nano Lett.* 14, 1021 (**2014**).
28. Z. F. Li, K. B. Alici, E. Colak, and E. Ozbay, *Appl. Phys. Lett.* 98, 161907 (**2011**).
29. E. Hendry, R. V. Mikhaylovskiy, L. D. Barron, M. Kadodwala, and T. J. Davis, *Nano Lett.* 12, 3640 (**2012**).
30. D. Lin and J. S. Huang, *Opt. Express* 22, 7434 (**2014**).
31. P. B. Johnson and R. W. Christy, *Phys. Rev. B* 6, 4370 (**1972**).

Received: 15 September 2015. Accepted: 25 September 2015.